Supporting Information for Engineering Hierarchical Porosity in MOFs for Host–Guest Chemistry with Large Organometallic Complexes

Jakob Blaschke [a], Maria Asghar [b], Zheao Huang [a], Stephen Nagaraju Myakala [a], Shaghayegh Naghdi [a], Thomas Schachinger [c], Hanspeter Kählig [d], Olga Lanaridi [e], Andreas Limbeck [e], Jérôme Durand [f], Philippe Serp [f,g], Florian Libisch [b], Dogukan H. Apaydin [a], Dominik Eder [a]**

[a] Institute of Materials Chemistry, TU Wien, Getreidemarkt 9/BC/02, 1060 Vienna, Austria. Email: dominik.eder@tuwien.ac.at; dogukan.apaydin@tuwien.ac.at

[b] Institute of Theoretical Physics, TU Wien, Wiedner Hauptstraße 8-10, 1040, Vienna, Austria

[c] University Service Centre for Transmission Electron Microscopy (USTEM), TU Wien, Wiedner Hauptstraße 8-10, 1040 Vienna, Austria

[d] Department of Organic Chemistry, Faculty of Chemistry, University of Vienna, Währinger Str. 38, 1090 Vienna, Austria

[e] Institute of Chemical Technologies and Analytics, TU Wien, Getreidemarkt 9, 1060 Vienna, Austria

[f] Laboratoire de Chimie de Coordination, UPR CNRS 8241, Composante ENSIACET, Université de Toulouse, UPS-INP-LCC, 4 Allée Emile Monso, BP 44362, 31030 Toulouse Cedex 4, France

[g] Institut Universitaire de France (IUF), 1 rue Descartes, F-75231 Paris, France

Experimental Details

Chemicals

For the synthesis of the metal-organic framework (MOF) materials, $ZrCl_4$ (abcr, 99.5%), terephthalic acid (BDC, Fluka, >99%), 2-amino-terephthalic acid (NH_2-BDC, Thermo scientific, 99%), concentrated acetic acid (Fisher chemical, 98-100%), concentrated HCl (Fluka, >37%) and N,N'-dimethylformamide (DMF, Thermo scientific, p.a., 99.5% / Extra Dry, 99.8%) were used without further purification. Furthermore, the chemicals and solvents needed for the complexation of the Re: 2,2'-bipyridine-4-carboxylic acid (BLD Pharmatech, 95+%), pentacarbonylchlororhenium(I) (Thermo scientific, 98%) and toluene (Fisher chemical, p.a., >99.8%) were also used as received.

Synthesis of UiO-samples

The synthesis of UiO and UiO_{NH2} was based on the optimized microwave assisted method developed by Taddei *et al.*[1] For this, $ZrCl_4$ (291 mg, 1.25 mmol) was dissolved in 10 mL of DMF under stirring in a beaker. Concentrated acetic acid (2.1 mL, 37.5 mmol) and deionized water (0.135 mL, 7.5 mmol) were added to the solution and an equimolar amount of linker was added as soon as the $ZrCl_4$ was fully dissolved. In the case of UiO only BDC (208 mg, 1.25 mmol) was added while for the sample $UiO_{NH2,}$ NH_2-BDC (23 mg, 0.125 mmol) was added before BDC (187 mg, 1.125 mmol). The mixtures had to be heated to 70 °C to speed up the dissolution of the BDC linker. After 15-30 minutes, the stir bar was removed and the clear solution was transferred into a microwave vial (G20), capped and placed into an Anton-Paar Monowave 300 microwave where the solution was heated to 120 °C with a hold time of 15 min without any stirring. After the reaction finished, white (UiO) or yellow solid (UiO_{NH2}) had precipitated from the solution. The vial was air cooled and the solid filtered and washed at least three times with fresh DMF, followed by another three washing steps with methanol. To exchange any remaining DMF solvent from the pores, the MOF powders were redispersed in

fresh methanol and left standing in it for 4 days during which the methanol was exchanged once. After the solvent exchange, the powders were separated from the solution via centrifugation and dried at 60 °C after which they were milled with a mortar and pestle and finally activated in a vacuum oven overnight at 120 °C. The final yield after activation was about 310 mg.

For the synthesis of UiO_{Ideal} the protocol developed by Shearer *et al*. was employed in which $ZrCl_4$ (3.78 g, 16.2 mmol) was dissolved in 97.4 mL of DMF in an Erlenmeyer flask under stirring. Concentrated HCl (37%, 2.865 mL, 32.45 mmol) was added to the solution and in contrast to the microwave synthesis protocol, an excess of BDC linker was used in this case (5.39 g, 32.4 mmol). The solution was split in half and placed in two 100 mL Teflon liners, which were sealed in a steel autoclave and placed in an oven pre-heated to 220 °C. After 24 h, the reactors were taken out and cooled rapidly using a water bath. The reaction was filtered, yielding a white powder, however, to remove the excess linker which was used, the sample was washed with DMF once and then redispersed in 160 mL of fresh DMF and left to stir at room temperature overnight. During the next day the sample was continually left to stir in DMF, exchanging the DMF twice with 80 mL of fresh solvent. After an additional 8 h of washing, the DMF was exchanged with 80 mL of fresh methanol and left to stir overnight. The next day the powder was washed one more time with fresh methanol, after which the sample was collected via centrifugation, dried at 60 °C and activated in a vacuum oven at a temperature of 140 °C, for 12 h.

SeLiRe process

For the selective removal of the NH_2-BDC ligands to form $UiO_{SeLiRe,}$ activated UiO_{NH2} was placed into a muffle oven in a ceramic crucible and heated to 310 °C with a heating rate of 5 °C/min and a holding time of 12 h. The sample turned from yellow to brown during this

process, most likely due to not fully oxidized reaction products from the removal of NH_2-BDC.[2]

Modification with bpy-4-COOH

To incorporate the bipyridine moieties into the framework, SALI was performed with all MOFs and 2,2'-bipyridine-4-carboxylic acid (bpy-4-COOH). Approximately 200 mg of the MOF samples were placed in a Schlenk-tube with a magnetic stirrer and capped with a septum. The samples were then activated over night by heating to 120 °C under vacuum for 16 h. After filling the tubes with Ar and weighing the samples again, 3 equivalents of bpy-4-COOH (calculated using the calculated molecular weight of the MOF, under consideration of the defects, UiO: 1447 g/mol, UiO_{NH2}: 1450 g/mol, UiO_{SeLiRe}: 1351 g/mol, UiO_{Ideal}: 1701 g/mol, approx. 85-90 mg) were dissolved in an amount of DMF so that the final mixture would have a loading of 40 mg/mL of MOF (approx. 5-7 mL). The dissolved bipyridine was added via a needle through the septum and the MOF was dispersed via stirring and holding the Schlenk tube into the ultrasonic bath for 1 min. After that the mixture was heated to 60 °C under stirring and kept at that temperature for 24 h. After the reaction, the powder was collected via centrifugation and washed with DMF and methanol at least 3 times each. After the final washing step, the powders were again redispersed in methanol and stirred overnight after which the solvent was removed and the powders were dried at 60 °C in preparation for the final step, the reaction with $[Re(CO)_5Cl]$. The samples were denoted as UiO-bpy, UiO_{NH2}-bpy, UiO_{SeLiRe}-bpy and UiO_{Ideal}-bpy.

Complexation with $Re(CO)_5Cl$

Before the $[Re(CO)_5Cl]$ was added, the samples were again activated by placing approx. 50 mg of UiO-bpy, UiO_{NH2}-bpy and UiO_{SeLiRe}-bpy into a Schlenk tube each with a magnetic stirrer and capped with a septum followed by heating the samples to 120 °C under vacuum for 16 h. The tubes were filled with Ar and the true mass of the MOF was evaluated. A stock solution

of [$Re(CO)_5Cl$] was prepared in hot toluene with a concentration of 6.6 mg/mL and 5 mL of the solution were added to each sample. After stirring the reaction at 90 °C for 24 h, the samples were filtered and washed with hot toluene and methanol at least three times and dried at 90 °C.

Characterizations

SEM measurements were performed on a JEOL JSM-7800F Prime FEGSEM device using an acceleration voltage of 5.0 kV and at a working distance of 6.0 mm. The dry powders were placed on sticky carbon tape and placed in the sample chamber and evacuated.

STEM images were recorded on a FEI/ThermoFisher Tecnai G2 F20 equipped with an X-FEG electron source and operated at 200 kV acceleration voltage. A small amount of powder was dispersed in ethanol by placing the suspension in an ultrasonic bath. Afterwards the suspension was drop-casted onto a Lacey-Carbon copper grid. The STEM-EDX mapping was acquired using a 30 mm^2 EDAX-AMETEK Apollo XLTW silicon drift detector.

Powder XRD diffractograms were recorded on a PANalytical X'Pert Pro multi-purpose diffractometer, equipped with a copper source (1.5406 Å) in Bragg-Brentano geometry. A few mg of powder were placed on a zero background Si sample holder and pressed flat using a glass microscope slide. The samples were inserted into the device which was equipped with an autosampler and the diffractograms were recorded between 2-50° using a step size of 0.0201° and measurement time of 22.925 s/step under rotation of the sample. The longer capillary measurements were performed on a PANalytical Empyrean diffractometer with a copper source by filling a capillary with an outer diameter of 0.3 mm with the sample and measuring the diffractogram from 2-12° under rotation of the capillary. The step size was 0.0143° and measurement time 1387.8 s/step averaging a total of 4 scans.

Digestion NMR was performed to quantify the organic components in the MOF by dissolving 2-4 mg of sample in 450 µL of 1M NaOH in D_2O directly inside an NMR tube. After shaking

the dispersion and placing the tube in an ultrasonic bath for 1 min, the sample was allowed to react for 24 h, after which the inorganic solids had collected at the bottom of the NMR tube, where they did not disturb the measurement. Spectra were recorded on a Bruker AVANCE 250 (250.13 MHz) with a 5 mm inverse probe head with Z-gradient averaging 64 scans each with a relaxation time of 2 s.

TGA measurements were done using a PerkinElmer Thermogravimetric Analyser TGA 8000. Approx. 2 mg of the sample were loaded into an Al_2O_3 crucible which was first weighed empty. Using a heating rate of 5 °C/min, the samples were heated from 30 to 700 °C under a constant flow of synthetic air (20 mL/min).

Argon and nitrogen adsorption measurements were performed to determine the textural properties of the materials. Argon isotherms were collected at 87 K on a Micromeritics 3Flex analyzer equipped with a CryoTune accessory, while nitrogen isotherms were measured at 77 K using the same instrument. Prior to analysis, the samples were degassed under vacuum at 120 °C for 12 h. The total pore volume was estimated from the adsorptive uptake at P/P_0 = 0.95, assuming negligible external surface contribution. BET surface areas were calculated following the criteria recommended for microporous materials.[3] Pore size distributions and micro/mesopore volumes were obtained from the adsorption branch of the isotherms using nonlocal density functional theory (NLDFT) assuming cylindrical pores on an amorphous SiO_2 surface, implemented in Micromeritics Flex v6.01 software.

Solid state nuclear magnetic resonance spectroscopy (ssNMR). All spectra were measured on a Bruker Avance NEO 500 MHz wide bore system (Bruker BioSpin GmbH & Co. KG, Ettlingen, Germany) using a 4 mm triple resonance magic angle spinning (MAS) probe. The resonance frequency for ^{13}C NMR was 125.78 MHz, the MAS rotor spinning was set to 14 kHz. Cross polarization (CP) was achieved by a ramped contact pulse with a contact time

of 3 ms. During acquisition ^{1}H was high power decoupled using SPINAL with 64 phase permutations. The chemical shifts are reported in ppm and are referenced external to adamantane by setting the low field signal to 38.48 ppm,

DRS measurements were performed on a Jasco V670 UV-Vis spectrometer equipped with an integrating sphere. The sample was pressed against a quartz window, and spectra were collected at 400 nm/min with 1 nm resolution.

Steady state PL measurements were performed on a PicoQuant FluoTime 300 spectrophotometer and using a Xe arc lamp (300 W power) as the excitation source. The excitation wavelength was set to 310 nm using a double-grating monochromator. A PMA Hybrid 07 in combination with another high-resolution double monochromator was used for the detector. The solid samples were measured in a solid sample holder positioned behind a quartz window and for the physical mixtures, the concentrations of the complex were set to match those of the synthetically modified samples.

FTIR-ATR measurements were performed on a Perkin Elmer Spectrum Two using the ATR inset UATR TWO by pressing the dry powders against the ATR crystal using a piston which applied a constant force. The spectra were recorded at a resolution of 4 cm^{-1} and averaging 4 scans.

For the LA-ICP-MS measurements, the MOF powders were dispersed in a 6 wt% polyvinylpyrrolidone (MW ~ 1.300.000, 1 mg sample in 5 mL) solution in ethanol and an internal In-standard was added after which the final concentration of PVP was adjusted to 5.4 wt% of PVP by adding ultra pure water. The samples were suspended in the PVP solution and vortexed (Vortex Genie 2, Scientific Industries). Subsequently, the suspension was ultrasonicated with the aid of an ultrasonication processor (UP400S, Hielscher, Germany), set at 75% amplitude and 12 kHz duty cycle, for 4 times, 60 sec each. During ultrasonication, the

container with the suspension was covered with aluminum foil to minimize solvent losses through evaporation. The resulting dispersion was spin coated with a KLM spin-coater SCV-10 (Schaefer-Tec, Germany) onto a 1x1 cm Si wafer (3600 RPM, 90 s, ≈ 75 µL of solution added after spinning axis had reached the desired rotational speed). The solvent was evaporated by placing the wafers on a heating plate at 60 °C, for 5 min. The concentration of the In-standard was set to 50 µg/g and for quantification a 6-point multi-element calibration curve was measured with data points between 5 and 1000 µg/g of Re and Zr. The concentrations refer to the final polymer films on the wafer. The actual measurements were performed using a Nd:YAG deep UV (213 nm) solid state laser (New Wave 213) by Elemental Scientific Industries Inc. The ablation chamber was coupled to an ICP-MS (iCAP-Q) by ThermoFisher Scientific, connected via PTFE tubing and using He as a carrier gas. For the ablation, a linear pattern (5 lines of 5 mm length with a distance of 150 µm) was applied across the wafer.

XAS measurements were performed at the BL14W1 beamline at the Shanghai Synchrotron Radiation Facility (SSRF) which is a third-generation hard X-ray absorption fine structure (XAFS) platform powered by a 38-pole wiggler source. It offers tunable photon energy ranging from 4.5 keV to 50 keV via Si(111) (4.5–18 keV) and Si(311) (8.5–50 keV) double crystal monochromators, enabling high-resolution measurements of Re L-edges (L_3-edge) within its optimal energy window. The beamline delivers a focused photon flux of $>1\times10^{13}$ phs/s at 10 keV (300 mA) with a beam size of 0.3×0.3 mm^2 (H×V) at the sample position, ensuring high signal-to-noise ratios for trace-element analysis. For X-ray detection a 32-element Canberra/XIA Germanium (Ge) detector was used. It features an energy resolution of 0.5×10^{-4} (at 10 keV, Si(311)) and fast count rate capability, minimizing spectral distortion from overlapping emissions. The detector is positioned at 90° to the incident X-ray beam to maximize fluorescence collection while suppressing elastic scattering. For Re L_3-edge fluorescence XAFS at SSRF BL14W1, a three-ionization-chamber setup is employed, with I_0/I_t

(90% N_2 + 10% Ar, 300 V) monitoring beam intensity and an optional He-filled chamber suppressing scattering, while a Si(311) monochromator with Rh mirror ensures high resolution

XPS spectra were recorded on a ThermoScientific K-Alpha system using a monochromatised Al Kα (hv = 1486.6 eV) source with an X-ray spot size of about 400 µm. The pass energy was set to 30 eV with a step size of 0.1 eV for detail spectra. For charge correction and energy calibration the adventitious carbon peak (C-C peak) was shifted to 284.8 eV binding energy (BE) and to reduce charging effects a broad-spot low energy flood gun was used for charge compensation. Data analysis was performed using CASA XPS software, employing transmission corrections (as per the instrument vendor's specifications) and Shirley/Tougaard backgrounds.[4,5]

Photocatalytic CO_2RR was conducted in a 10 mL sealed batch reactor with a water-cooled mantle and a 365 nm UV-LED (Thorlabs SOLIS-365C, 0,264 W/cm² power density). MOF (6 mg) was ultrasonically dispersed in 2.0 mL DMF:TEOA (5:1 v/v), transferred to the reactor with a stir bar, and sealed with a septum. The suspension and headspace were purged with 100% CO2 (≥20 mL/min, ≥20 min) via two needles. The reactor was placed in a dark enclosure, stirred at ~500 rpm, and maintained at 15 °C by a recirculating chiller. After 1 h illumination, headspace gases were quantified by GC (Shimadzu GC-2030, BID, Micropacked-ST column). To verify the source of carbon for the detected products, several control experiments were performed: (i) solvent only; (ii) unmodified MOFs without Re-modification; (iii) homogeneous reference with dissolved Re complex [Re(bpy-4-COO^-)CO_3Cl] in an amount matching the Re loading of UiO_{SeLiRe}-Re (0.8 mg /1.6 µmol in 2 mL of solvent); (iv) no CO_2: the dispersion was bubbled with Ar gas instead of CO_2; (v) no light: the solution was bubbled with CO_2, but the lamp was not turned on and the headspace was sampled after 1 h in the dark; (vi) no TEOA: the MOF was dispersed in DMF only. Furthermore, a long-term experiment using UiO_{SeLiRe}-Re (6 mg) and the homogeneously dissolved complex (0.8 mg) were conducted where the

samples were illuminated over a duration of approx. 21 h and the headspace was sampled regularly. In order to calculate the TOF and TON, the amount of Re was quantified by using the results from LA-ICP-MS and estimating the molecular weight from the TGA/NMR results (see "Determination of MOF composition").

Determination of MOF composition

The combination of TGA and digestion NMR can be used to determine the sum formula and cluster composition of a MOF sample. For a full and detailed discussion see the excellent publications by Shearer *et al.* and Sannes *et al.* [6,7] In short, the analysis relies on the assumption that the final decomposition product is ZrO_2 which is normalized to 100% in the TGA graph. Additionally, there is a plateau before the final weight loss step where the composition of the MOF is known. For UiO_{Ideal} there is a plateau around 400 °C where the sample only contains the dehydroxylated clusters and linkers ($Zr_6O_{6+x}(BDC)_{6-x}$ - modulators and solvents have already been removed and charges are compensated by O^{2-}). An ideal UiO-66 sample would have a sum formula of $Zr_6O_6(BDC)_6$ and would exhibit a weight loss of 120.2% when being converted to ZrO_2 (based on ZrO_2 weight).

$$W_{Plateau,\ ideal} = \left(\frac{M_{dehydroxylated\ MOF}}{M_{final\ product}}\right) * 100\% = \left(\frac{M_{Zr_6O_6(BDC)_6}}{M_{6\ ZrO_2}}\right) * 100\% = \left(\frac{1628.0\frac{g}{mol}}{739.3\frac{g}{mol}}\right) * 100$$

From the ideal plateau $W_{Plateau,\ ideal}$ the theoretical weight loss per linker can be calculated by dividing the total weight loss by the number of linkers.

$$WL_{linker} = \frac{W_{Plateau,\ ideal} - 100\%}{\#linkers_{ideal}} = \frac{220.2\% - 100\%}{6} = 20.03\%$$

Differences between the ideal and the experimental plateau are attributed to missing linker defects and by dividing the actual experimental final weight loss step by the weight loss per linker ($^{WL_{linker}}$) the actual number of linkers can be calculated.

$$\#linkers_{experimental} = 6 - x = \frac{W_{plateau,\,experimental} - 100\%}{WL_{linker}} = \frac{W_{plateau,\,experimental} - 100\%}{20.03\%}$$

In the case of a mixed-linker MOF such as UiO_{NH2}, the calculation must be modified with the theoretical molecular weight of the mixed-linker MOF. For determination of the ratio of NH_2-BDC to the total amount of linkers, the results from digestion NMR are needed. The relative quantification of NH_2-BDC/BDC from the peak integrals can be converted to the NH_2-BDC/Linker ratio under the assumption that only these two linkers are present in the MOF. In the case of UiO_{NH2} the ratio of NH_2-BDC/Linker is 0.11 which means the theoretical sum formula of a dehydroxylated, defect-free sample is $Zr_6O_6(NH_2\text{-}BDC)_{0.66}(BDC)_{5.34}$.

$$W_{Plateau,\ ideal} = \left(\frac{M_{dehydroxylated\ MOF}}{M_{final\ product}}\right) * 100\% = \left(\frac{1638.0\frac{g}{mol}}{739.3\frac{g}{mol}}\right) * 100\% = 221.6\%$$

$$WL_{linker} = \frac{W_{Plateau,\ ideal} - 100\%}{\#linkers_{ideal}} = \frac{221.6\% - 100\%}{6} = 20.26\%$$

$$\#linkers_{experimental} = 6 - x = \frac{W_{plateau,\,experimental} - 100\%}{20.26\%}$$

To get the number of linkers per cluster, the result must be multiplied by 2 since the sum formula only has 6 linkers in total in an ideal UiO-66 type MOF.

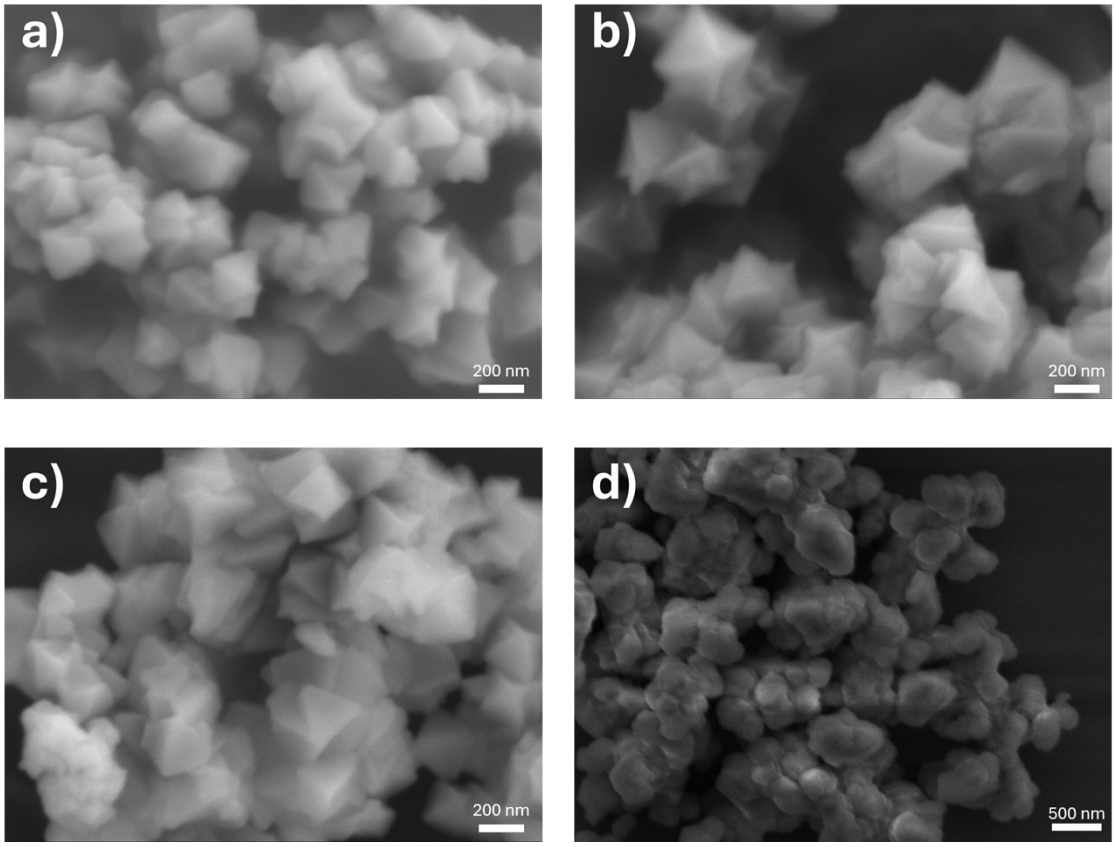

Figure S1. SEM images of a) UiO, b) UiO_{NH2}, c) UiO_{SeLiRe} and d) UiO_{Ideal}. The three defectious samples show octahedral, partially intergrown particles with an average diameter of approximately 200 nm, while UiO_{Ideal} exhibits an irregular morphology and a larger particle size of approx. 500 nm. Importantly, also the selective ligand removal process did not lead to a significant change in morphology of the particles, indicating that the framework remains stable upon thermally removing a small fraction of ligands.

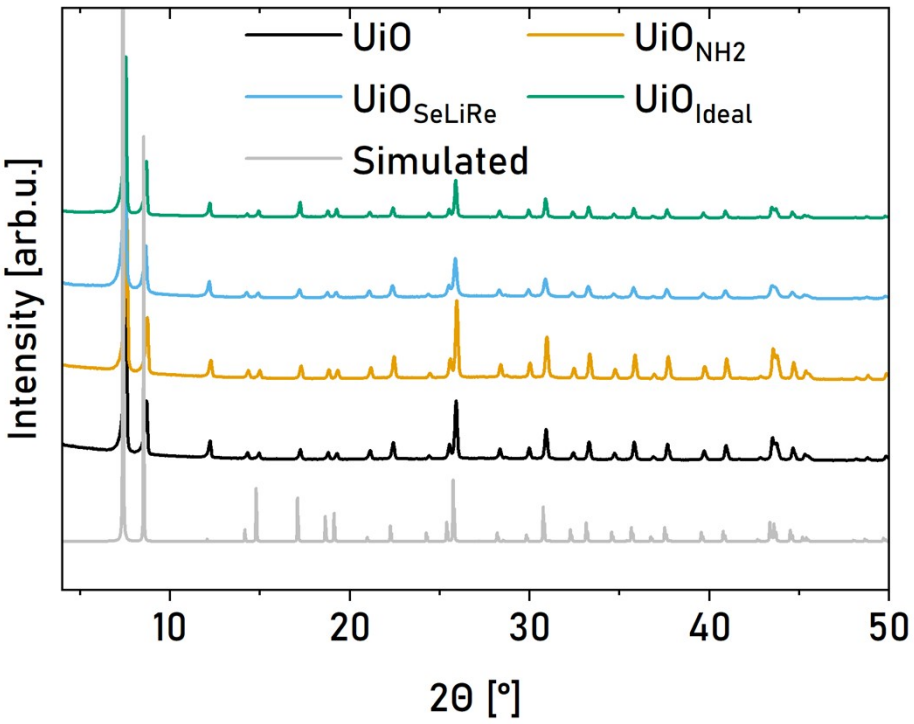

Figure S2. Powder XRD patterns of the 4 base samples and a simulated pattern of UiO-66. All samples are crystalline and show all relevant peaks for the UiO-66 phase.

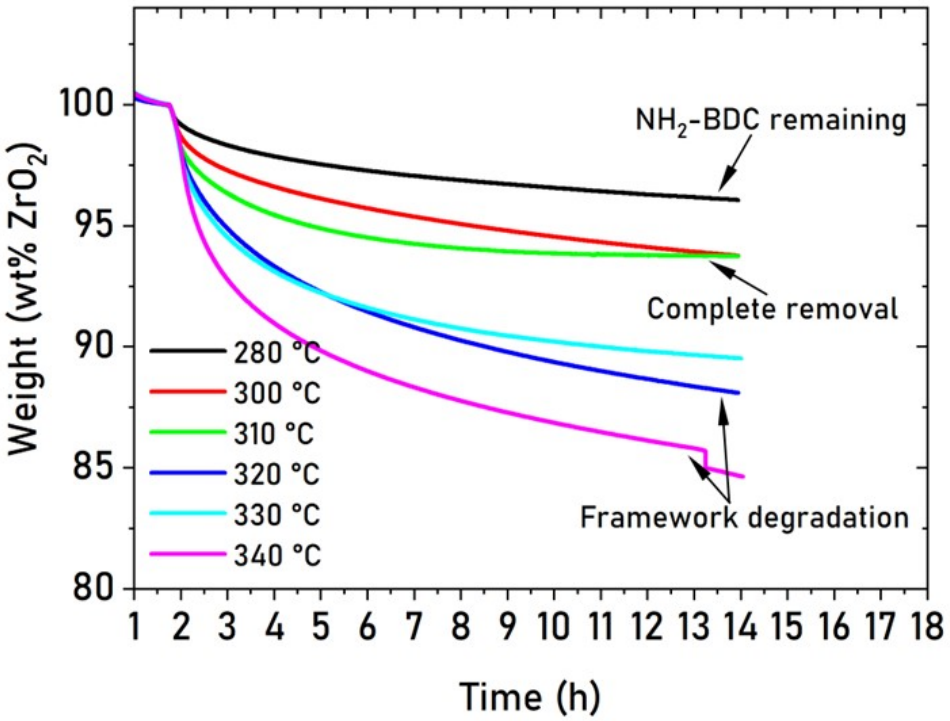

Figure S3. Isothermal TGA curves for UiO_{NH2} with a holding time of 12 h at different temperatures. During the first two hours, the samples were heated to 250 °C to remove physisorbed water and solvents from the pores. Lower holding temperatures such as 280 °C led to an incomplete removal of the NH_2-BDC; the TGA curve is still sloping downwards after the total degradation time of 12 h. Higher degradation temperatures lead to a further attack of the framework and degradation of the BDC linkers. At a temperature of 310 °C after 12 h a stable TGA curve could be achieved, indicating the complete removal of NH_2-BDC and simultaneous stability of the BDC linkers.

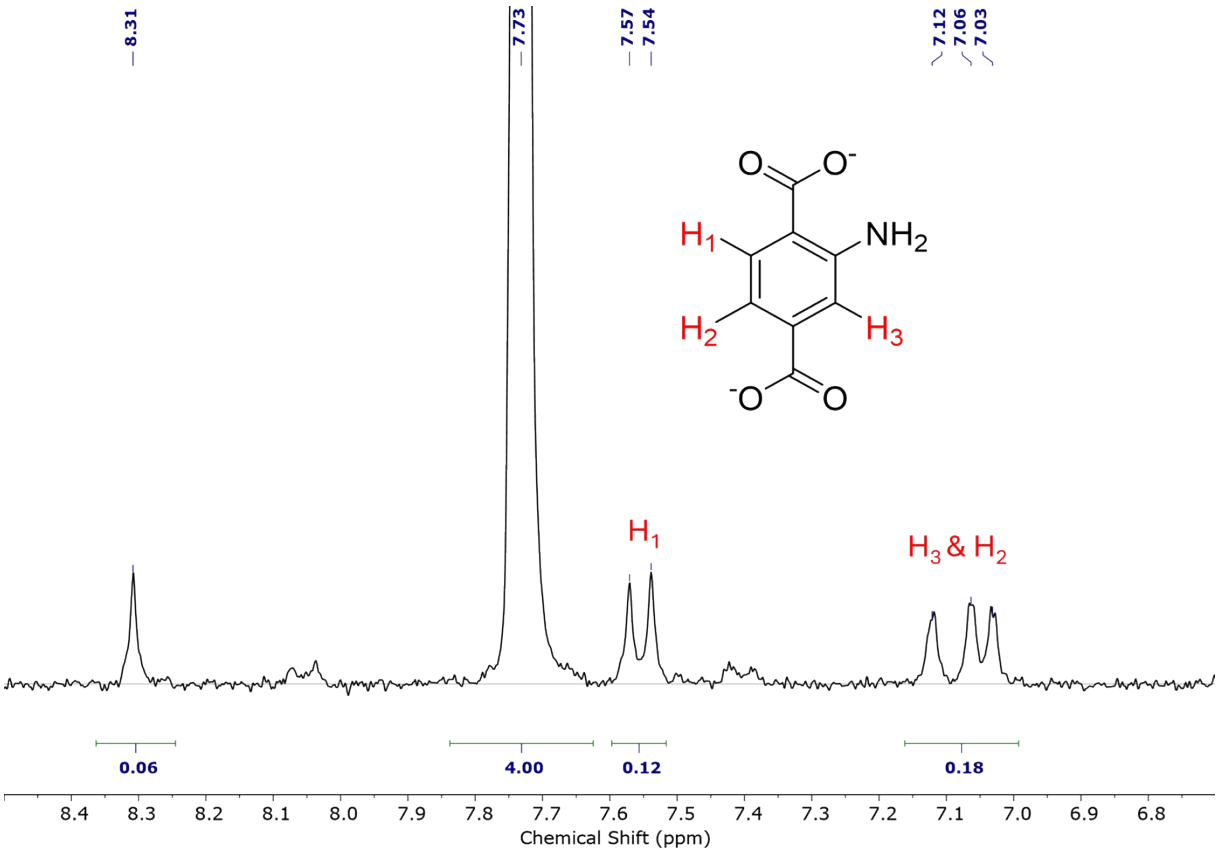

Figure S4. ^{1}H-NMR signal integration of UiO_{NH2}. The total linker ratio was calculated from the relative signals of BDC^{2-} and NH_2-BDC^{2-}. For the calculation, the signal of H_1 was selected and while NH_2-BDC/BDC is equal to 0.12, the ratio of NH_2-BDC to the total linkers constitutes 11%, which fits well with the intended ratio of 10%.

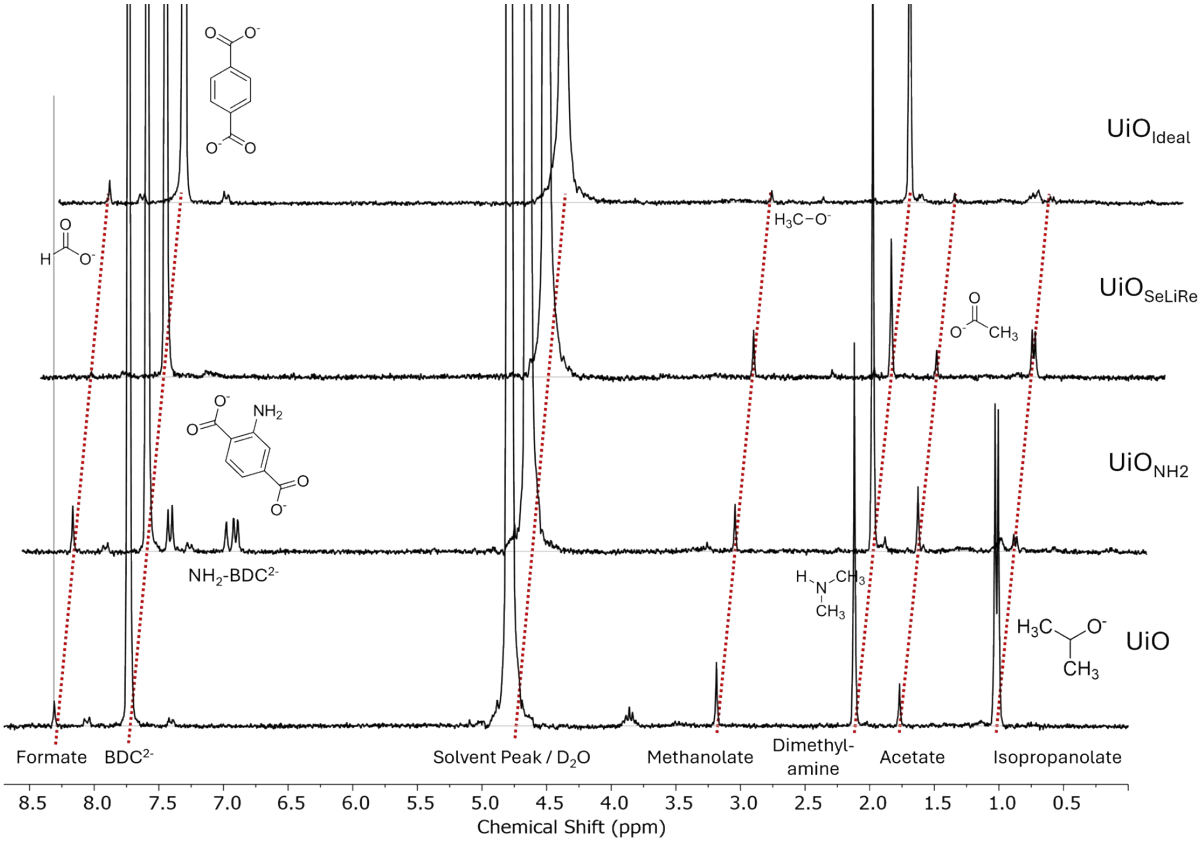

Figure S5. Full ^{1}H-NMR spectra of the 4 parent samples showing both the aromatic and aliphatic ^{1}H region. In the aromatic region the signals of the linkers BDC^{2-} and NH_2-BDC^{2-} are visible with an additional peak for formate. Dimethylamine is generated in situ during the synthesis from the decomposition of DMF and acetate was used in the synthesis as a modulator. Methanol was used for washing the sample after synthesis and isopropanol was absorbed from the lab atmosphere due to the high porosity of the samples.

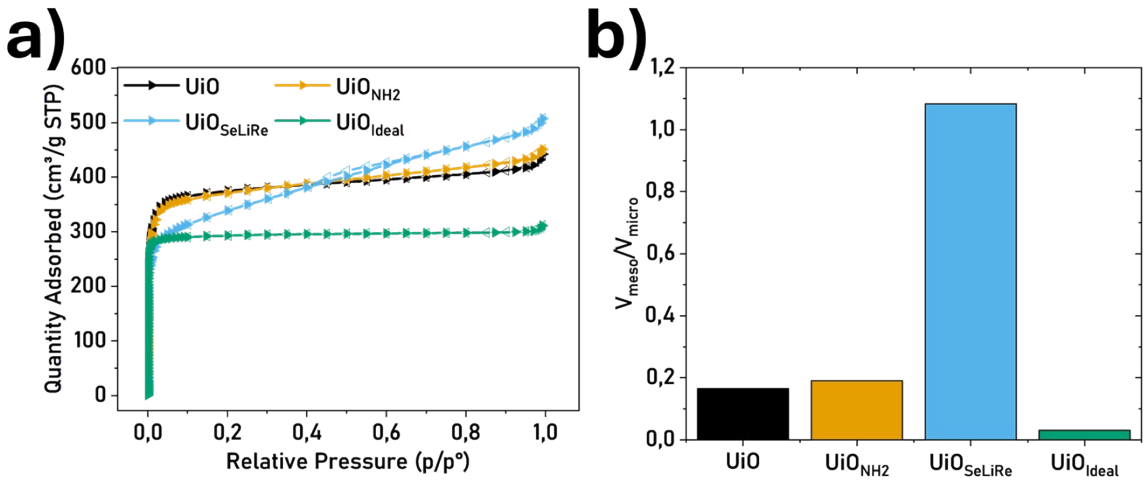

Figure S6. a) N_2-isotherms (77 K) recorded for the four base samples. While UiO, UiO$_{NH2}$ and UiO$_{Ideal}$ all show mostly flat isotherms, UiO$_{SeLiRe}$ exhibits a slope in the isotherm as well as a small hysteresis hinting at pore condensation and mesoporosity. The results match well with the Ar-physisorption data. b) Ratio of total mesopore volume and total micropore volume calculated from the t-plots of the samples. UiO$_{SeLiRe}$ shows a strongly increased mesopore ratio.

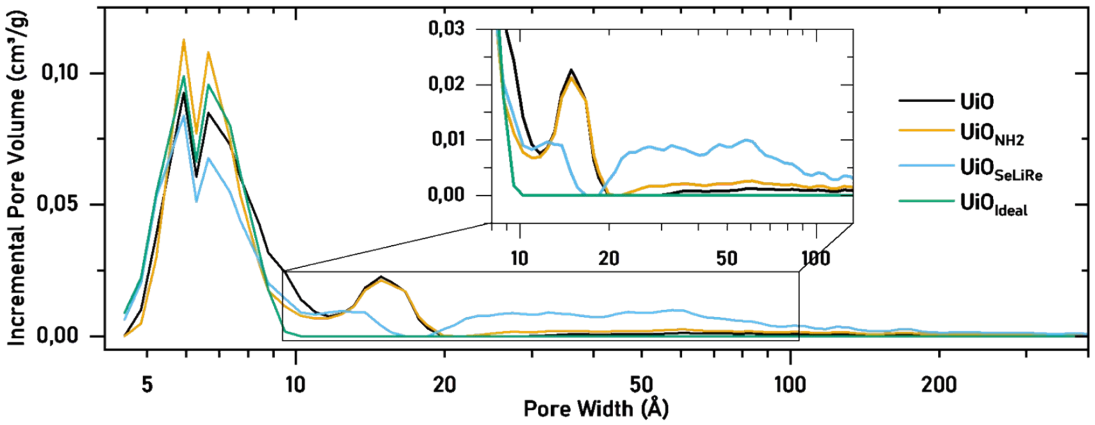

Figure S7. NLDFT pore distribution calculated from the N_2-isotherms. All samples show a large peak around 6 Å while the three defect rich samples show an additional peak around 15 Å, which was assigned to the MC defects with a missing linker sphere. UiO$_{SeLiRe}$ also shows an increased amount of mesopores.

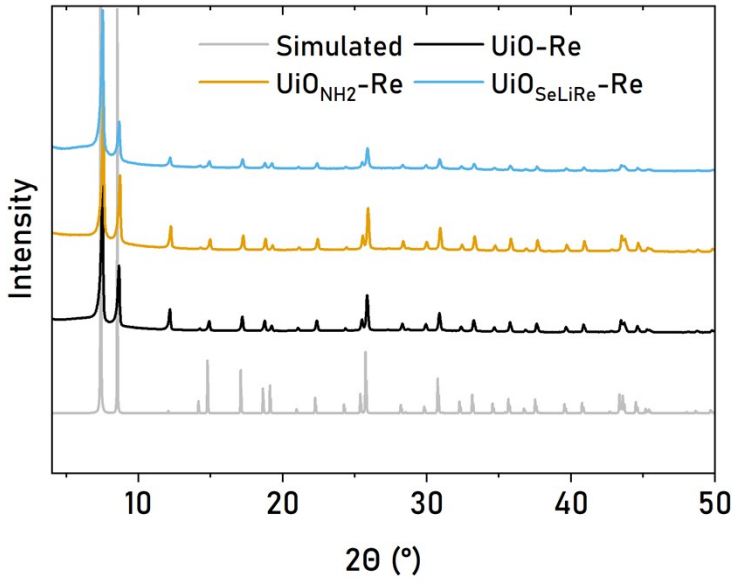

Figure S8. PXRD diffractograms of the Re-modified samples compared with the simulated UiO-66 pattern. all three samples exhibit the expected UiO-66 peaks and no additional peaks from a crystalline [Re(bpy-4-COOH)(CO)$_3$Cl] phase.

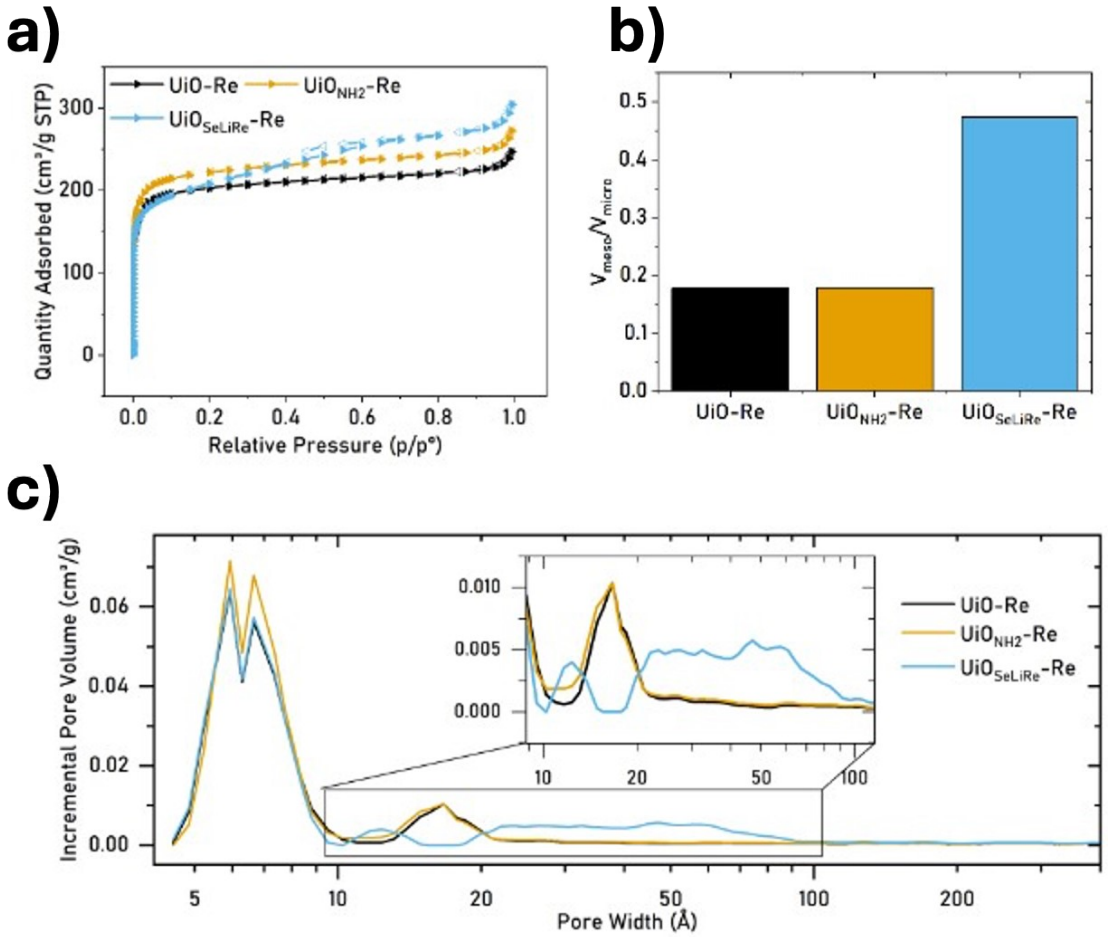

Figure S9. a) N_2-physisorption isotherms (77 K) for the Re-modified samples UiO-Re, UiO_{NH2}-Re and UiO_{SeLiRe}-Re. Like the unmodified samples, UiO-Re and UiO_{NH2}-Re show mostly flat isotherms, while UiO_{SeLiRe}-Re still exhibits a sloped isotherm and hysteresis due to mesopores, which persist after the Re-modification. b) t-plots and c) NLDFT pore distribution of the modified samples, showing the same pores as the unmodified samples.

Table S1. BET surface areas of the four base samples and Re-modified samples calculated from the N_2-physisorption and Ar-physisorption isotherms.

Sample	Surface Area (N_2-physisorption) [m²/g]	Surface Area (Ar-physisorption) [m²/g]
UiO	1511	1048

UiO_{NH2}	1477	1292
UiO_{SeLiRe}	1254	1037
UiO_{Ideal}	1180	1096
UiO-Re	798	-
UiO_{NH2}-Re	872	-
UiO_{SeLiRe}-Re	772	-

Table S2. TGA-plateaus for all samples, as well as the calculated connectivities, NMR-quantification of the bpy-4-COOH incorporation into the samples as well as the resulting number of bipyridines per Zr_6-cluster and the molar Re/Zr ratio from the LA-ICP-MS analysis.

Sample	TGA plateau [wt% ZrO_2]	# of linkers / Zr_6-cluster	NMR-ratio bpy-4-COOH/BDC	# of bpy-4-COOH / Zr_6-cluster	Molar ratio (Re/Zr)	# of Re / Zr_6-cluster
UiO	189%	8.9	0.08	0.39	0.065	0.39
UiO_{NH2}	186%	8.5	0.05	0.20	0.062	0.37
UiO_{SeLiRe}	180%	8.0	0.10	0.46	0.071	0.43
UiO_{Ideal}	219%	11.8	0.00	0.00	-	-

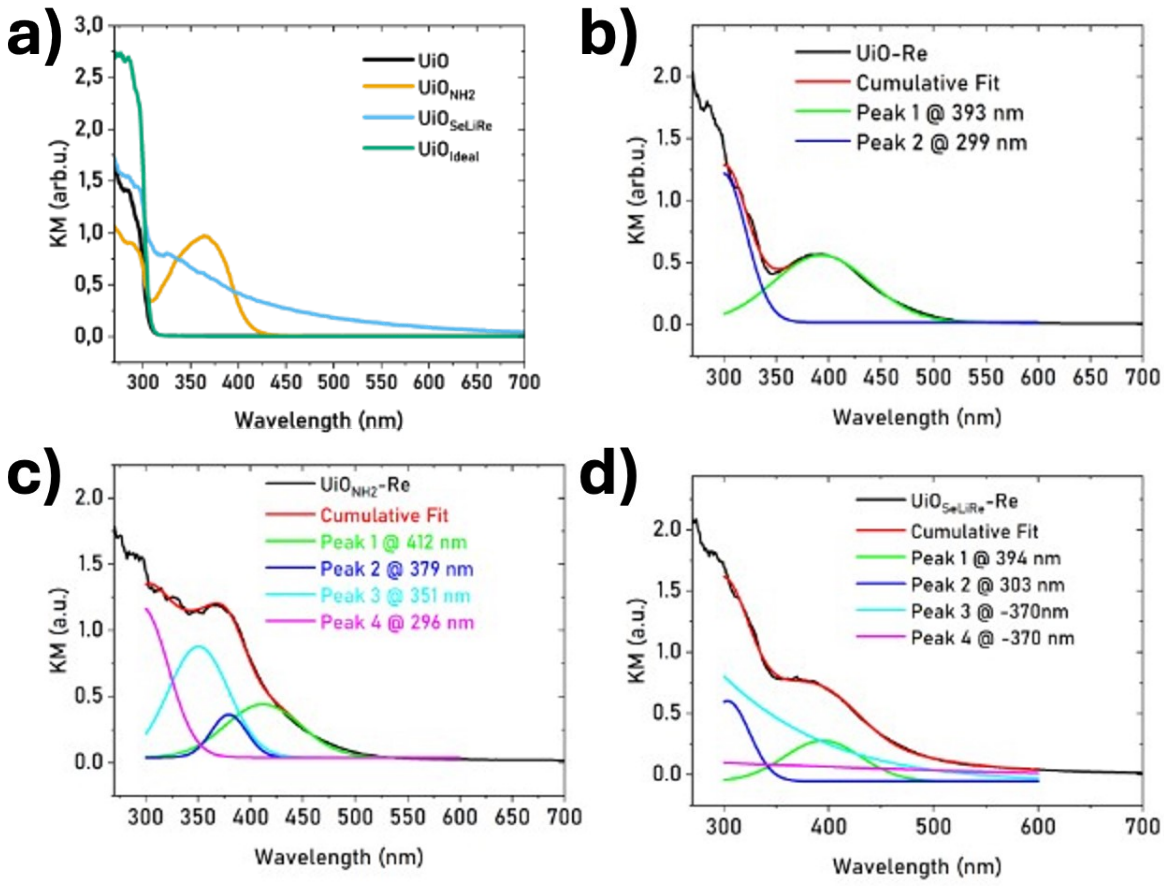

Figure S10. a) DRS spectra of the four base samples. b)-d) Re-modified samples UiO-Re, UiO_{NH2}-Re and UiO_{SeLiRe}-Re with fitted peaks to determine the peak position of the Re-complex absorption. The samples were fitted with Gauss peaks from 300-600 nm. Peak 1 always corresponds to the MLCT transition of the Re-complex in the MOF. The rest of the peaks were chosen after fitting the unmodified samples and transferring the parameters to the new fit. UiO_{SeLiRe} was fitted with two peaks with negative center positions, because the base sample showed a constantly decreasing absorption, sloping downwards toward higher wavelengths and not a defined absorption.

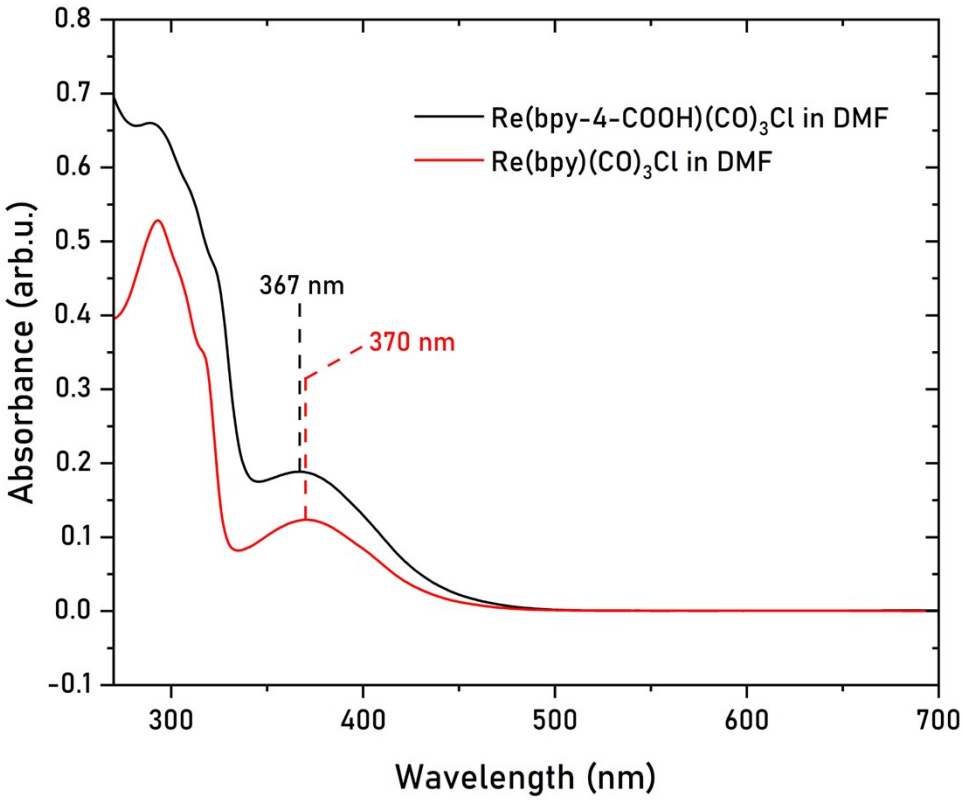

Figure S11. UV-Vis absorbance spectra of $Re(bpy\text{-}4\text{-}COOH)(CO)_3Cl$ and $Re(bpy)(CO)_3Cl$ for comparison at a concentration of 0.1 mM in DMF. Both complexes show almost the same absorbance spectrum with only a slight shift in the MLCT visible.

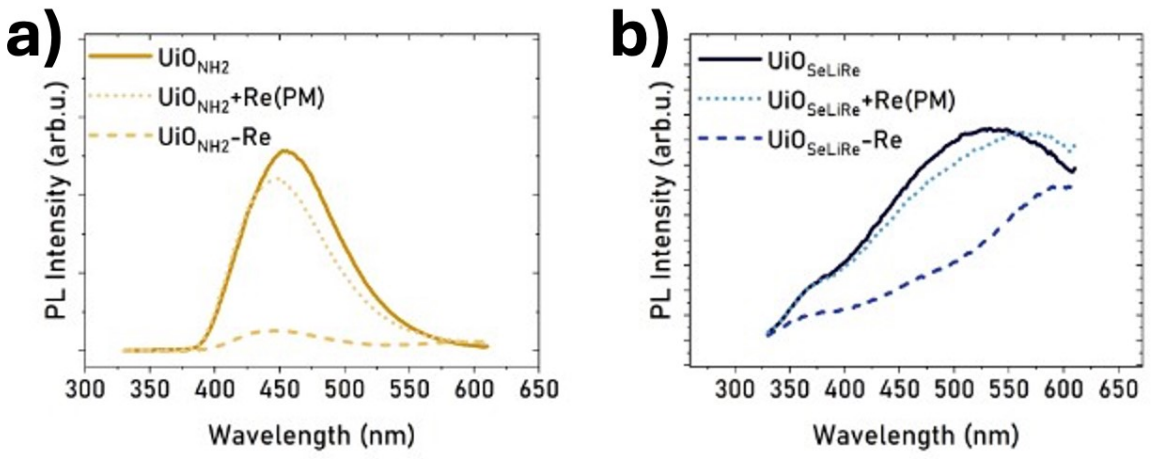

Figure S12. PL emission spectra after excitation with 310 nm of a) UiO_{NH2} and b) UiO_{SeLiRe}. Both samples show the same behavior of luminescence quenching as in UiO when the sample

is modified with Re hinting at an electron transfer from the MOF to the Re-complex. The quenching is not as pronounced when the sample is merely physically mixed with the complex Re(bpy-4-COOH)$(CO)_3$Cl. In the case of UiO_{NH2} the sample shows a different emission maximum at around 460 nm compared to UiO due to the presence of the NH_2-BDC linkers in the framework. The UiO_{SeLiRe} sample shows a large emission at 525 nm and a shoulder at 358 nm which corresponds to the main UiO luminescence also observed in the UiO sample.

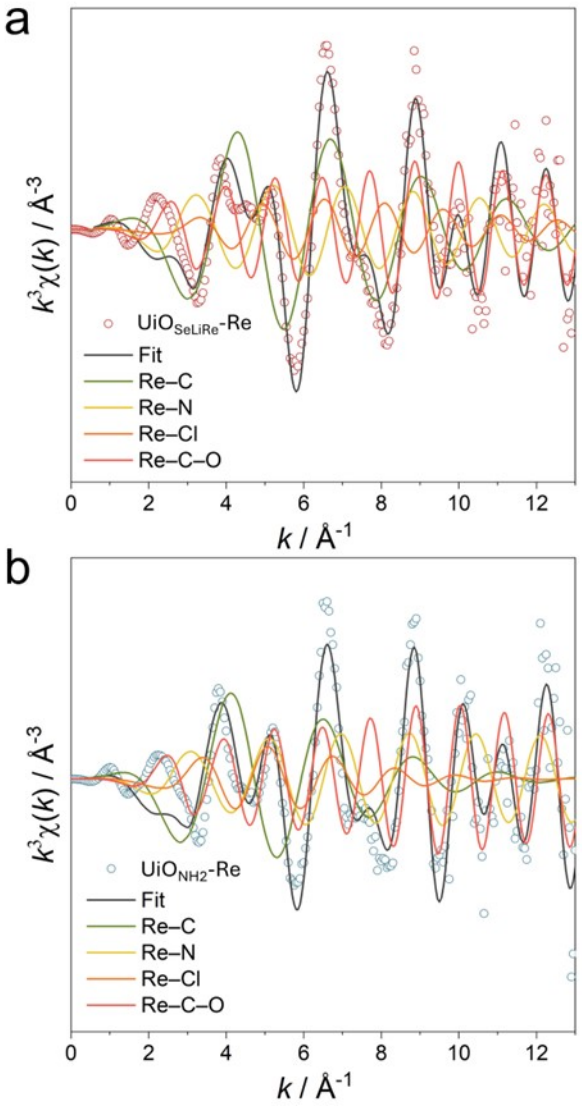

Figure S13. a, b) Fourier-transformed (FT)-EXAFS $k^3\chi(k)$ oscillations of UiO_{NH2}-Re and UiO_{SeLiRe}-Re in k-space and their corresponding multi-shell fitting.

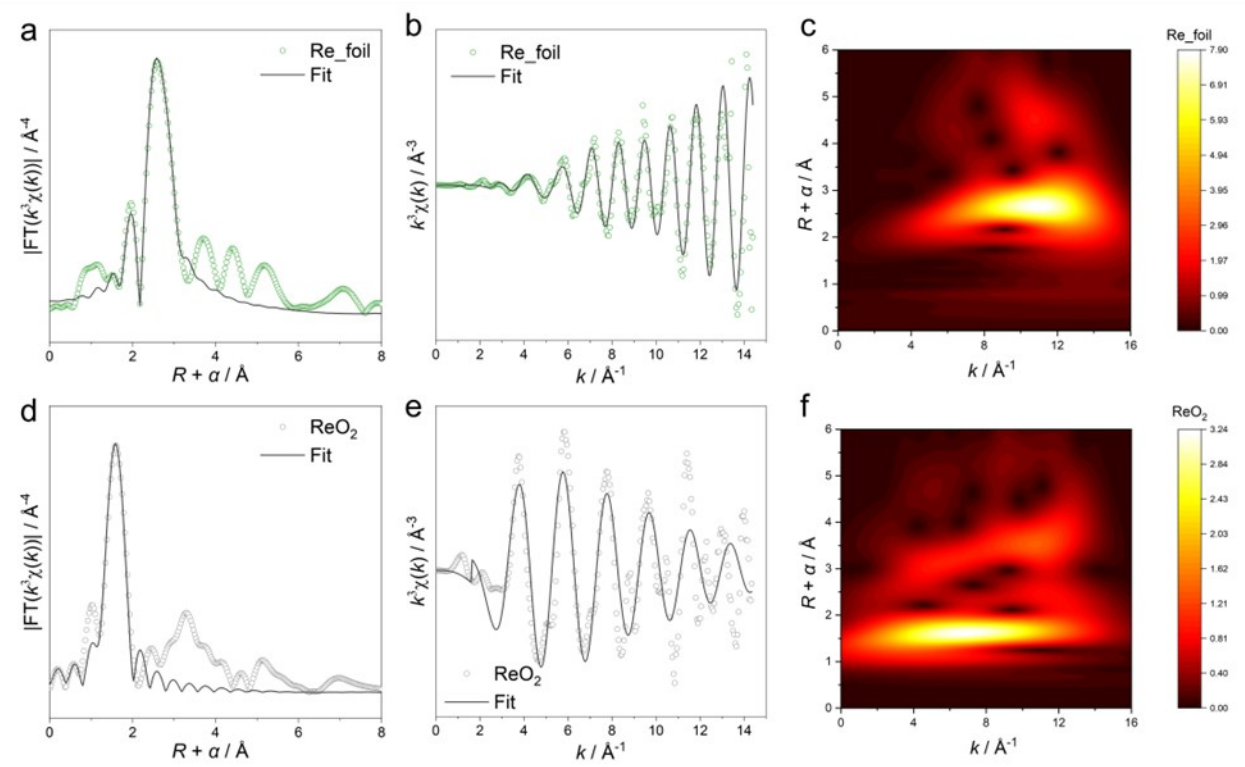

Figure S14. Re L_3-edge EXAFS analysis of Re foil (a–c) and ReO_2 (d–f). Fourier-transformed (FT)-EXAFS k^3-weighted $\chi(k)$ function spectra in R-space (a, d), the corresponding $k^3\chi(k)$ oscillations in k-space (b, e), and the Wavelet transforms (WT) contour plots (c, f).

Table S3. Structural parameters extracted from the quantitative fitting of the Re L_3-edge EXAFS data (S_0^2=0.9).

Samples	Paths	CN[a]	R (Å)[b]	σ^2 (Å^2)[c]	ΔE_0 (eV)[d]	R factor[e]
Re foil	Re–Re	12	2.74±0.01	0.0031	0.7±0.1	0.0086
ReO_2	Re–O	4.9±0.3	1.98±0.01	0.0044	9.98±1.63	0.0146
UiO_{SeLiRe}-Re	Re–C	2.8±0.4	1.74±0.02	0.0067	1.28±4.04	0.0134
	Re–N	2.4±0.9	2.17±0.02	0.003		
	Re–Cl	0.8±0.5	2.45±0.05	0.0062		
	Re–C–O	5.3±1.1	3.13±0.03	0.001		
UiO_{NH2}-Re	Re–C	3.9±0.5	1.77±0.02	0.0138	-1.48±2.88	0.0197
	Re–N	2.0±0.6	2.18±0.01	0.0005		
	Re–Cl	1.9±1.0	2.38±0.05	0.0183		

	Re–C–O	5.0±0.7	3.11±0.01	0.0002

[a]CN: coordination number; [b]R: bond distance; [c]σ^2: Debye-Waller factor; [d]ΔE_0: inner potential correction. R-factor: goodness of fit. The error bounds characterizing the structural parameters obtained by EXAFS spectroscopy were estimated as CN±20%; R ± 1%; σ^2 ± 20%.

The XAS data were processed using Athena (version 0.9.26) for background subtraction, pre-edge, and post-edge line calibrations. Subsequent Fourier transform and EXAFS fitting were carried out in Artemis (version 0.9.26). To obtain an unbiased assessment of the local coordination environments and prevent parameter correlation, the data were fitted by freely floating the coordination numbers (CN) for all paths. The only constraint applied during the refinement was to the Debye-Waller factors (σ^2). For the fitting of UiO_{SeLiRe}-Re, a k^3-weighting, a k-range of 3–11 $Å^{-1}$, and an R-range of 1–3.1 Å were employed. For UiO_{NH2}-Re, the fitting was performed using k^3-weighting, a k-range of 3.5–12.5 $Å^{-1}$, and an R-range of 1–3.2 Å.

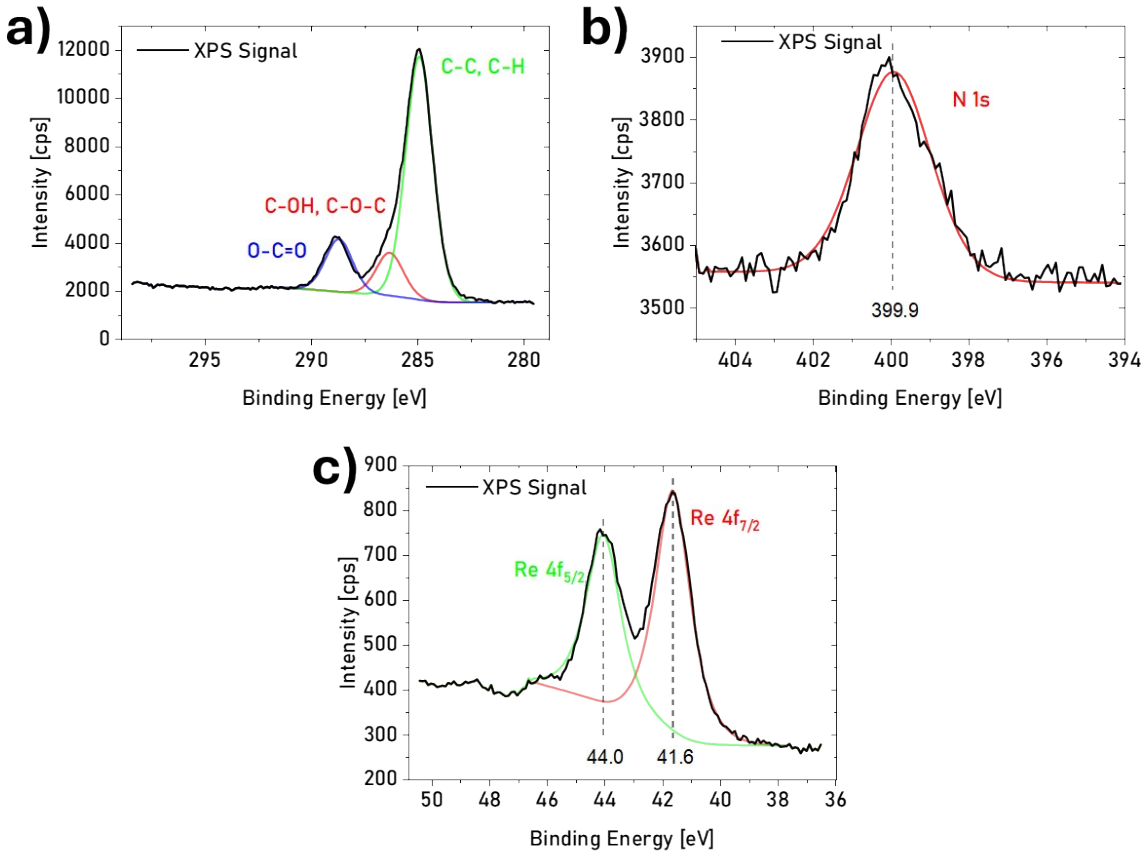

Figure S15. Detail XPS spectra of the a) C1s, b) N1s and c) Re4f regions for the sample UiO_{SeLiRe}-Re. While the C1s region shows the typical peaks for adventitious carbon, it also shows a high intensity for the O-C=O carbon peak which are present in the MOF. The N1s region shows a single peak at 399.9 eV. This most likely corresponds to the nitrogen from the bipyridine in the MOF and is shifted toward higher binding energies, compared to typical aromatic Ns.[8] This could be indicative of complex formation, where the interaction with Re pulls electrons from the nitrogen, increasing the binding energy of the 1s electron. The positions of the two Re signals match well with the expected positions of the $4f_{5/2}$ (44.0 eV) and Re $4f_{7/2}$ (41.6 eV) orbitals of Re(I) confirming that the Re oxidation state didn't change during complex formation.[9,10]

Computational details

For all calculations, we used the FHI-AIMS code package [11], with the default light Gaussian basis sets for H, C, O, Cl, and Zr, with PBE0 [12] as exchange functionals. To correctly account for the electrostatic environment within solution (and within the MOF), we employed a non-periodic boundary (cluster) calculation including the MultiPole Expansion (MPE-nc) implicit solvation model.[13] The relaxed geometries (within PBE0 after pre-relaxation with PBE) with periodic boundaries for Orientation-1 and -2 are shown in Figure S16. Further extensions of the clusters with two BDC-linkers were also considered and are shown in Figure S17. To elucidate the role of excited states, we also performed linear-response time-dependent density functional theory (LR-TDDFT) calculations[14] using FHI-AIMS for the Re-complex [Re(bpy)$(CO)_3$Cl], which can be seen in Figure S18.

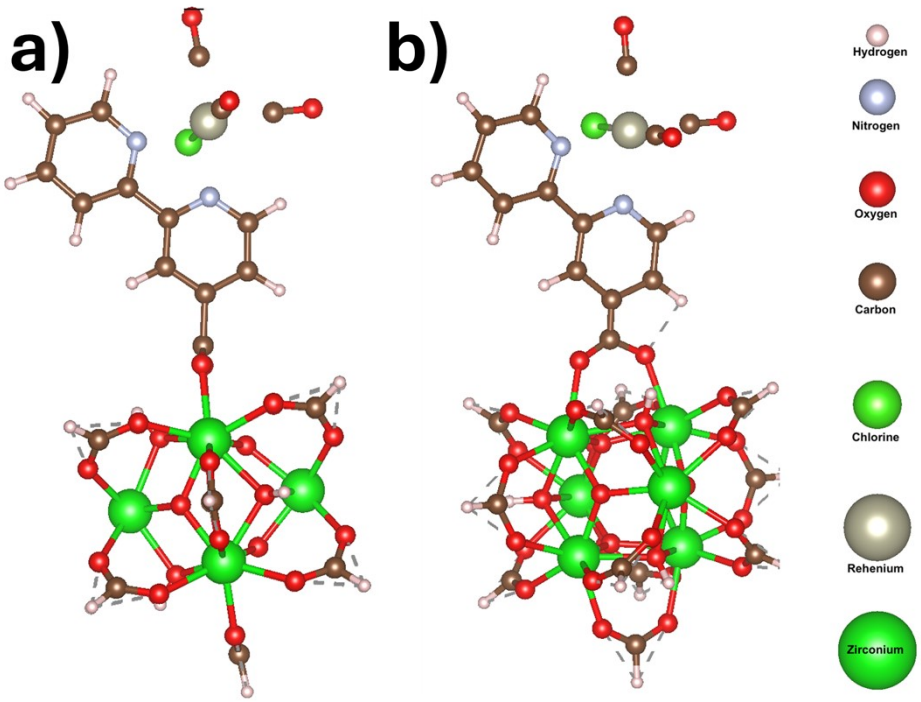

Figure S16. The relaxed geometries of Orientation-1(a) and Orientation-2 (b) with PBE0 functional.

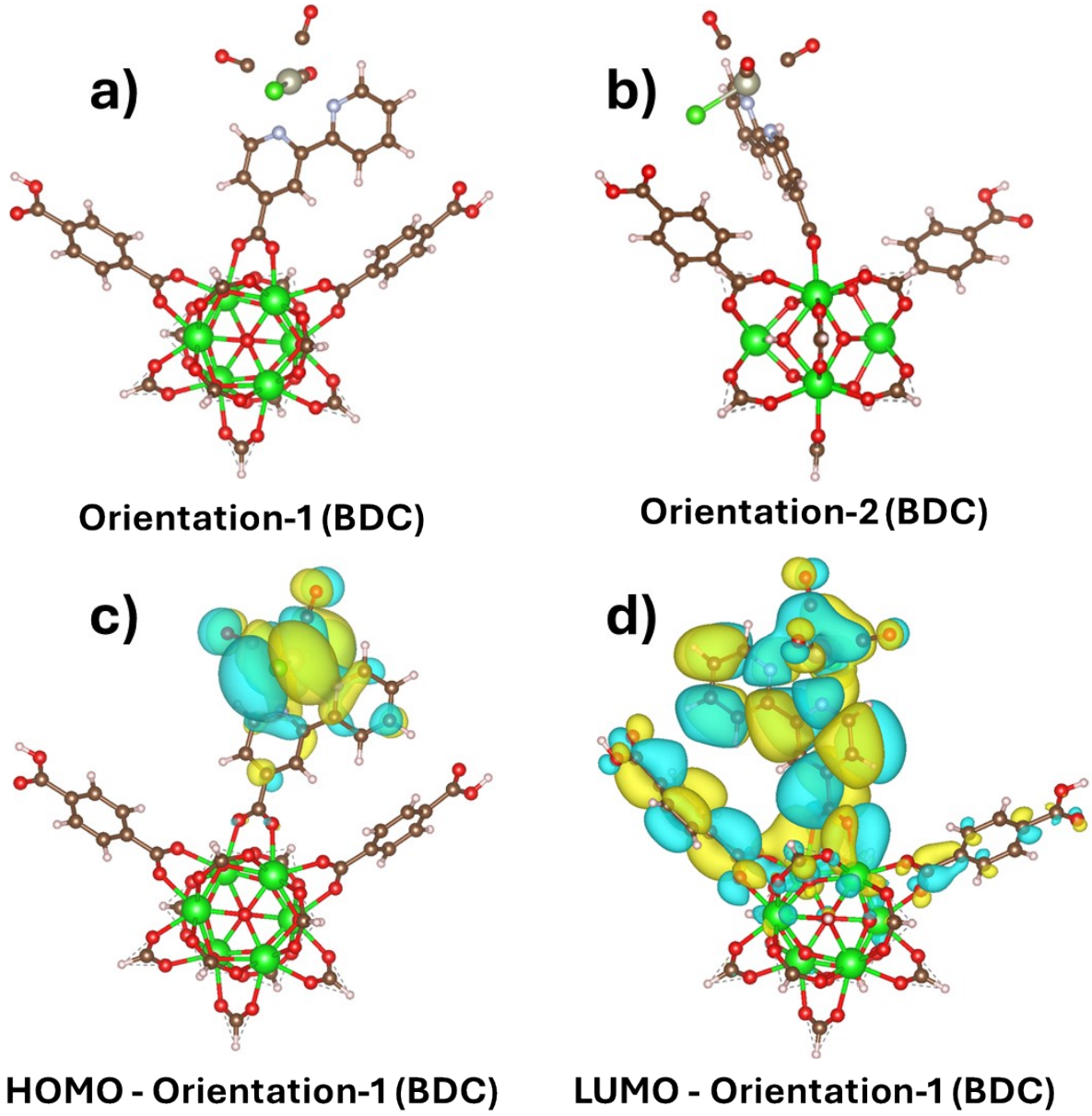

Figure S17. The relaxed geometries of the Zr_6-cluster with two attached BDC-linkers in a) Orientation-1 and b) Orientation-2 relaxed with PBE0 functional. c) and d) show the isodensity plots (at 0.003) of the HOMO and LUMO orbitals of Orientation-1 with two BDC linkers attached. Yellow and blue iso-surface parts correspond to two different signs of the wavefunction at the same density value. Compared to the isodensity plots of the cluster, fully capped with formate, the LUMO extends further along the carbon π-system of the ligands.

Table S4. The HOMO and LUMO orbital energies of Orientation-1 (BDC) and Orientation-2 (BDC), both with two attached BDC linkers; wavelengths from λ(nm) = 1240/E(eV).

Sample	HOMO (eV)	LUMO (eV)	Gap (eV)	Gap (nm)	Experimental values
Orientation-1 (BDC)	-5.96	-3.03	2.93	423	393 nm
Orientation-2 (BDC)	-6.03	-3.16	2.87	432	

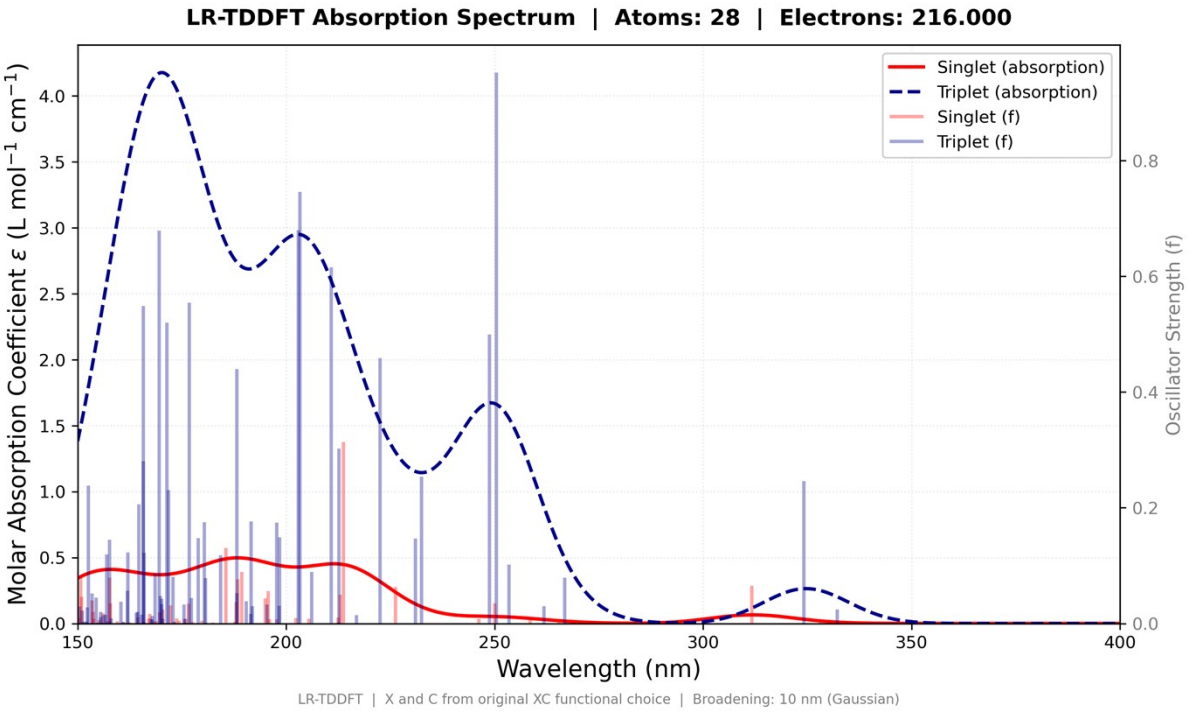

Figure S18. The absorption spectra of Re Complex using LR-TDDFT at PBE0 with FHI-AIMS.

Energy levels and orbital analysis for Orientation-2 and additional boundary conditions

Table S5. The total energies (in eV) and Fermi energies (in eV) of the relaxed geometries of different sets of Orientation-1 and Orientation-2, relative to the lowest energy (Orientation-2, without periodic boundaries).

	Orientation-1			**Orientation-2**		
	With periodic boundaries	**Without periodic boundaries**	**With solvation (DMF)**	**With periodic boundaries**	**Without periodic boundaries**	**With solvation (DMF)**
Total energy (eV)	0.08	0.07	0.28	1.00	0.00	0.23
Fermi energy (eV)	-4.96	-4.46	-4.76	-5.52	-4.59	-4.86

Table S6. The HOMO and LUMO orbital energies of Orientation-1, wavelengths from λ(nm) = 1240/E(eV).

Orientation-1	**HOMO (eV)**	**LUMO (eV)**	**Gap (eV)**	**Gap (nm)**	**Experimental values (nm)**
With periodic boundaries	-6.50	-3.42	3.08	403	393
Without periodic boundaries	-5.98	-2.94	3.04	408	393
With solvation (DMF)	-6.50	-3.01	3.51	353	393

Table S7. The HOMO and LUMO orbital energies of Orientation-2, wavelengths from λ(nm) = 1240/E(eV).

Orientation-2	HOMO (eV)	LUMO (eV)	Gap (eV)	GAP (nm)	Experimental values (nm)
With periodic boundaries	-6.78	-4.25	2.53	490	393
Without periodic boundaries	-6.02	-3.16	2.86	433	393
With solvation (DMF)	-6.51	-3.21	3.30	376	393

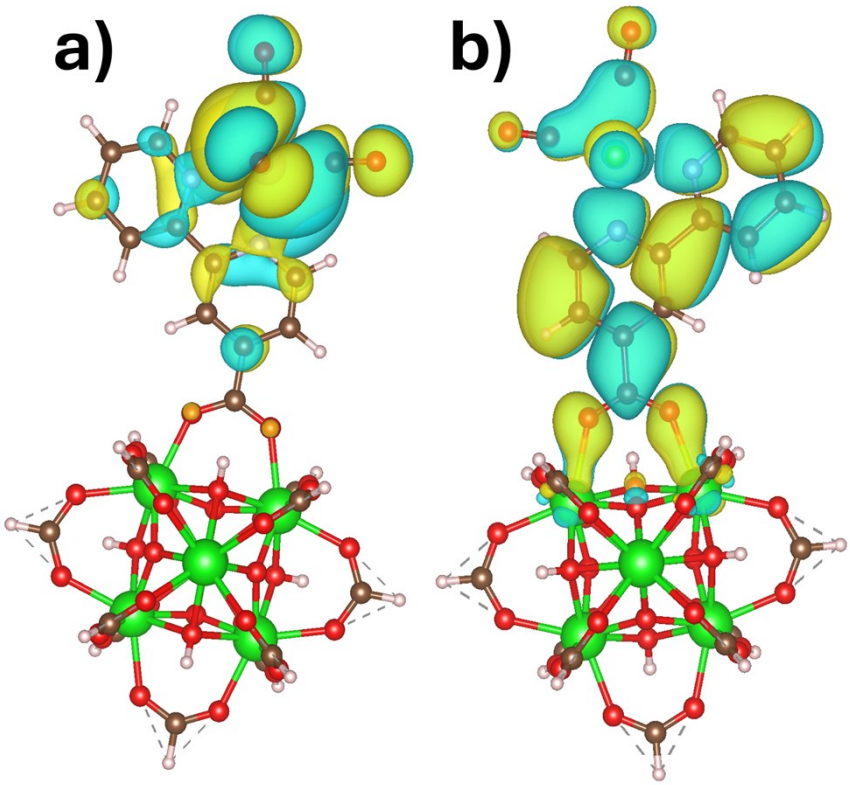

Figure S19. Isodensity plots of Orientation-2 for (a) the HOMO orbital and (b) the LUMO orbital (isosurface value of 0.003) without solvation. Blue and yellow refer to opposite signs of the orbital wavefunction.

Mulliken charge analysis

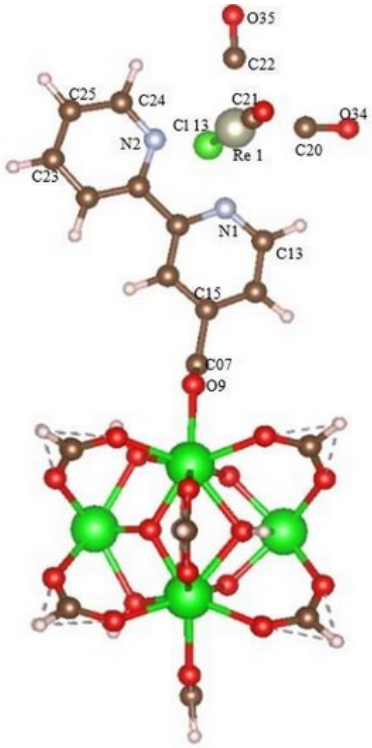

Figure S20. The relaxed geometry of Orientation-1. Atoms featuring notable charge transfer upon complexation in Mulliken charge analysis are labelled for comparison to Table S5 and Table S6.

Table S8. Mulliken charge analysis (in units of elementary charge) of selected atoms in the solvated Re-complex and of Orientation-1 (unsolvated).

Atom – Orientation-1	Re-complex (in sol)	Orientation-1 (no sol)	Difference
Cl	-0.55	-0.52	0.03
Re	-0.11	-0.12	-0.01
N1 (bpy)	-0.28	-0.28	0.00
N2 (bpy)	-0.28	-0.28	0.00
C34 (CO, Re-complex)	0.28	0.26	-0.02
O35 (CO, Re-complex)	-0.23	-0.22	-0.01

C15 (bpy, attachment point)	-0.07	-0.02	0.05

Table S9. Mulliken charge analysis (in units of elementary charge) of selected atoms in the solvated Re-complex and of Orientation-2 (unsolvated).

Atom – Orientation-2	Re-complex (in sol)	Orientation-2 (no sol)	Difference
Cl	-0.55	-0.60	-0.05
Re	-0.11	-0.12	-0.01
N1 (bpy)	-0.28	-0.27	0.01
N2 (bpy)	-0.28	-0.28	0.00
C34 (CO, Re-complex)	0.28	0.26	-0.02
O35 (CO, Re-complex)	-0.23	-0.23	0.00
C15 (bpy, attachment point)	-0.07	-0.06	0.01

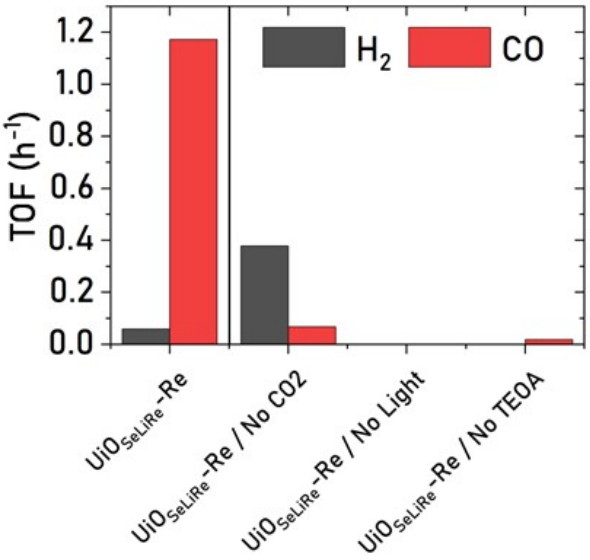

Figure S21. H_2 and CO TOF for the control experiments (i) with Ar instead of CO_2, (ii) in the dark and (iii) without the addition of TEOA as a sacrificial agent.

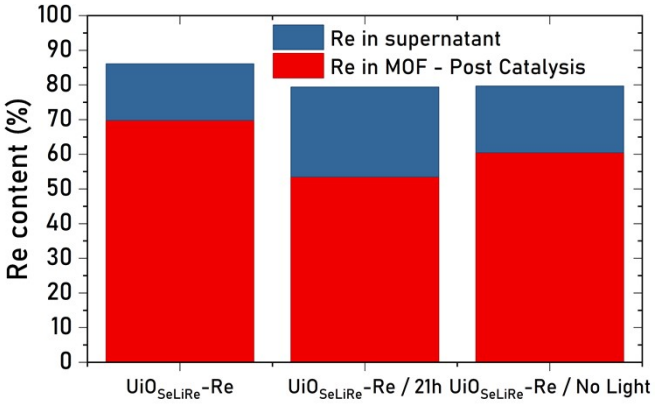

Figure S22. Post catalysis Re quantification in the MOF and supernatant, indicating that in all cases, most of the Re remains in the solid. The amount of leached Re only increases slightly after illuminating the catalyst for 21 h, also showing the long-term stability of the MOF under these conditions. The reason for the fact that the percentages do not add up to 100% is ascribed to difficulties in weighing in an exact amount of MOF for the catalytic experiment.

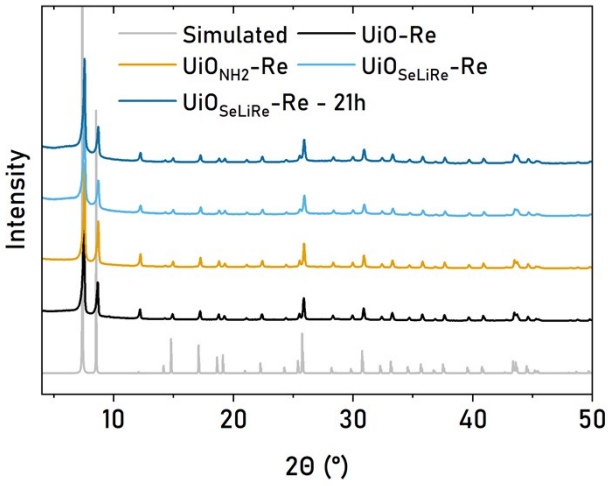

Figure S23. Post-catalysis PXRD diffractograms for the 1 h CO_2RR experiments of UiO-Re, UiO$_{NH2}$-Re, UiO$_{SeLiRe}$-Re and the 21 h experiment with UiO$_{SeLiRe}$-Re showing the stability of the MOFs under the conditions of photocatalytic CO_2RR.

References

1. Taddei M, Dau PV, Cohen SM, et al. Efficient microwave assisted synthesis of metal–organic framework UiO-66: optimization and scale up. *Dalton Trans*. 2015;44(31):14019-14026. doi:10.1039/C5DT01838B

2. Feng L, Yuan S, Zhang LL, et al. Creating Hierarchical Pores by Controlled Linker Thermolysis in Multivariate Metal–Organic Frameworks. *J Am Chem Soc*. 2018;140(6):2363-2372. doi:10.1021/jacs.7b12916

3. Sánchez-Varretti FO, García GD, Ramirez-Pastor AJ, Romá F. A simple model for studying multilayer adsorption of noninteracting polyatomic species on homogeneous and heterogeneous surfaces. *J Chem Phys*. 2009;130(19):194711. doi:10.1063/1.3139301

4. Shirley DA. High-Resolution X-Ray Photoemission Spectrum of the Valence Bands of Gold. *Phys Rev B*. 1972;5(12):4709-4714. doi:10.1103/PhysRevB.5.4709

5. Tougaard S. Universality Classes of Inelastic Electron Scattering Cross-sections. *Surf Interface Anal*. 1997;25(3):137-154. doi:10.1002/(SICI)1096-9918(199703)25:3<137::AID-SIA230>3.0.CO;2-L

6. Shearer GC, Chavan S, Bordiga S, Svelle S, Olsbye U, Lillerud KP. Defect Engineering: Tuning the Porosity and Composition of the Metal–Organic Framework UiO-66 via Modulated Synthesis. *Chem Mater*. 2016;28(11):3749-3761. doi:10.1021/acs.chemmater.6b00602

7. Sannes DK, Øien-Ødegaard S, Aunan E, Nova A, Olsbye U. Quantification of Linker Defects in UiO-Type Metal–Organic Frameworks. *Chem Mater*. 2023;35(10):3793-3800. doi:10.1021/acs.chemmater.2c03744

8. Xue F, Zhang J, Ma Z, Wang Z. Copper Dispersed Covalent Organic Framework for Azide–Alkyne Cycloaddition and Fast Synthesis of Rufinamide in Water. *Small*. 2024;20(25):2307796. doi:10.1002/smll.202307796

9. Greiner MT, Rocha TCR, Johnson B, Klyushin A, Knop-Gericke A, Schlögl R. The Oxidation of Rhenium and Identification of Rhenium Oxides During Catalytic Partial Oxidation of Ethylene: An In-Situ XPS Study. *Z Für Phys Chem*. 2014;228(4-5):521-541. doi:10.1515/zpch-2014-0002

10. Popov DA, Luna JM, Orchanian NM, Haiges R, Downes CA, Marinescu SC. A 2,2'-bipyridine-containing covalent organic framework bearing rhenium(I) tricarbonyl moieties for CO2 reduction. *Dalton Trans*. 2018;47(48):17450-17460. doi:10.1039/C8DT00125A

11. Blum V, Gehrke R, Hanke F, et al. *Ab initio* molecular simulations with numeric atom-centered orbitals. *Comput Phys Commun*. 2009;180(11):2175-2196. doi:10.1016/j.cpc.2009.06.022

12. Adamo C, Barone V. Toward reliable density functional methods without adjustable parameters: The PBE0 model. *J Chem Phys*. 1999;110(13):6158-6170. doi:10.1063/1.478522

13. Filser J, Reuter K, Oberhofer H. Piecewise Multipole-Expansion Implicit Solvation for Arbitrarily Shaped Molecular Solutes. *J Chem Theory Comput*. 2022;18(1):461-478. doi:10.1021/acs.jctc.1c00834

14. Liu C, Kloppenburg J, Yao Y, et al. All-electron ab initio Bethe-Salpeter equation approach to neutral excitations in molecules with numeric atom-centered orbitals. *J Chem Phys*. 2020;152(4):044105. doi:10.1063/1.5123290